Purdue University
Purdue e-Pubs

International Refrigeration and Air Conditioning
Conference

School of Mechanical Engineering

2016

Thermodynamic Properties of Low-GWP Refrigerant for Centrifugal Chiller

Masato Fukushima
AGC Chemicals, ASAHI GLASS Co.,Ltd, Japan, masato-fukusima@agc.com

Hiroki Hayamizu
AGC Chemicals, ASAHI GLASS Co.,Ltd, Japan, hiroki.hayamizu@agc.com

Mai Hashimoto
AGC Chemicals, ASAHI GLASS Co.,Ltd, Japan, mai-hashimoto@agc.com

Follow this and additional works at: http://docs.lib.purdue.edu/iracc

Thermodynamic properties of low-GWP refrigerant for Centrifugal Chiller

Masato FUKUSHIMA[1*], Hiroki HAYAMIZU[1], Mai HASHIMOTO[1]

[1]AGC Chemicals, Research & Development Division, ASAHI GLASS CO., LTD.,
10 Goikaigan, Ichihara, Chiba 2908566, Japan
e-mail: masato-fukusima@agc.com

ABSTRACT

Thermodynamic properties of HCFO-1224yd($CF_3CF=CHCl$), including critical parameters, vapor-liquid coexistence curve, vapor pressure and PVT properties, were determined experimentally. The measurements of vapor-liquid coexistence curve in the critical region were made through visual observation of the disappearance of meniscus at the vapor-liquid interface within an optical cell. The vapor pressure and the PVT properties were made using the constant-volume method. The saturated liquid densities were obtained by the method using pyrex glass floats. The critical density was determined as $530\pm5kg/m^3$. The critical temperature was determined $429.18\pm0.05K$ as the saturation temperature corresponding to the critical density. The critical pressure was determined by extrapolation of the vapor pressure measurements to the critical temperature as $3.380\pm0.005MPa$.

1. INTRODUCTION

In refrigeration and air-conditioning industry, HFCs refrigerants such as HFC-134a, HFC-245fa, R-410A and R-404A were developed as CFCs or HCFCs alternative refrigerants which have Ozone depletion Potential (ODP). But HFCs have high global warming potential (GWP), there are urgent needs to reduce HFCs emissions. Internationally, North America proposes to capture the gradual reduction of HFCs in the Montreal Protocol Meeting, which is for the purpose of protecting the ozone layer. In Europe, HFCs are regulated by the F-gas regulation and Mobile Air-Conditioning systems (MAC) Directive. On the other hand, in Japan, the revision of the part of act on Ensuring the Implementation of Recovery and Destruction of Fluorocarbons concerning Designated Products is determined, and this revision is going to be enforced on April 1st, 2015. To replace high GWP refrigerants, Low-GWP refrigerants are currently in development. HCFO-1224yd has the good characters such as low-GWP, non-flammable, low-toxicity, good-chemical and thermal suitability, good-compatibility with oil and equipment components (Fukushima et al, 2015). HCFO-1224yd has similar thermal properties to HFC-245fa, so it is suitable to use as the refrigerant to alternate HFC-245fa and HCFC-123 for centrifugal chiller, organic Rankine cycle system, heat pumps. In this study, we present measurements of the thermodynamic properties of HCFO-1224yd.

2. EXPERIMENTAL

2.1 Vapor-liquid coexistence curve near the critical region

The vapor-liquid coexistence curve near the critical region has been measured by the observation of meniscus disappearance. Figure 1 shows a schematic diagram of the apparatus. The main portion of apparatus includes an optical cell, expansion vessel and supplying vessel. These three vessels were connected to each other by three valves. The measurements were made by visual observation of the disappearance of the meniscus at the vapor-liquid interface within the optical cell. The temperature measurements were conducted with 25-ohm platinum resistance thermometer calibrated to ITS-90 with an aid of a thermometer bridge. The sample density was determined as the sample mass weight divided by the inner volume of the optical cell, the expansion vessel and the supplying vessel. These values were calibrated by filling water with known density under room temperature conditions, and were corrected with respect to the thermal expansion and pressure deformation. The experimental uncertainties of temperature and density were estimated within ± 20 mK and ± 3 kg/m^3, respectively.
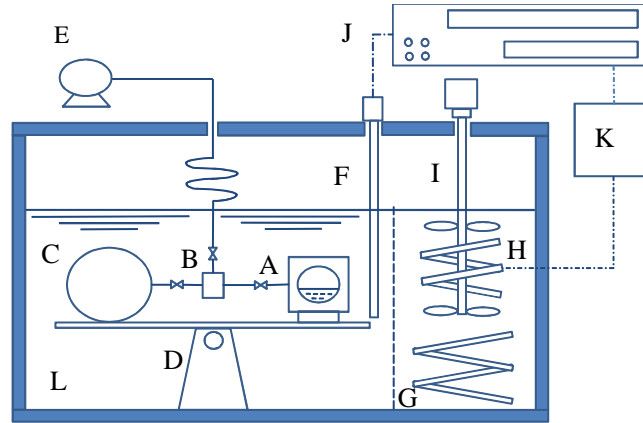
A: Optical cell   B: Expansion vessel   C: Supplying vessel   D: Rocking frame   E: Vacuum pump
F: Platinum resistance thermometer   G: Main-heater   H: Sub-heater   I: Stirrer
J: Thermometer bridge   K: PID controller   L: Thermostated bath
Figure 1: Schematic diagram of the apparatus for Vapor-liquid coexistence curve near the critical region

2.2 Vapor pressure and PVT properties

The vapor pressure and PVT properties have been measured by the constant volume method. Figure 2 shows a schematic diagram of the apparatus. The spherical sample vessel was made of 304 stainless steel. The differential pressure detector was connected with the sample vessel to separate the sample fluid from the nitrogen gas in the pressure transmitting system by a stainless steel membrane, and the whole setup was immersed into a thermostat bath. After confirming the established thermal equilibrium between the sample and the bath fluid, the temperature and pressure were measured by the methods which are mentioned Sec. 2.1. The pressure was measured by digital pressure indicators and a differential pressure gauge. The experimental uncertainties of temperature, pressure and density were estimated within $\pm$ 10 mK, $\pm$ 3 kPa and $\pm$ 0.2 %, respectively.
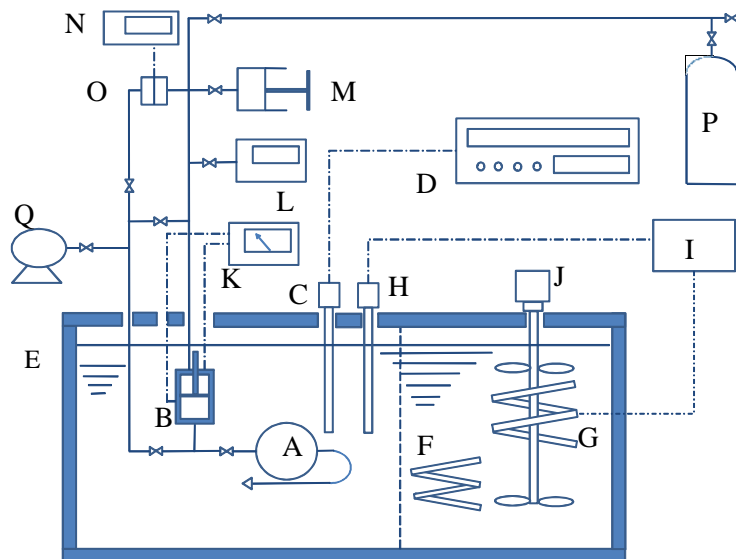
A: Vessel   B: Differential pressure detector   C: Platinum resistance thermometer   D: Thermometer bridge
E: Thermostat bath   F: Main-heater   G: Sub-heater   H: Platinum resistance thermometer
I: PID controller   J: Stirrer   K: Tester   L: Digital pressure gage   M: Pressure controller
N: Digital pressure gage   O: Differential pressure detector Q: Vacuum pump   P: N2 bottle
Figure 2: Schematic diagram of the apparatus for Vapor pressure and PVT properties

2.3 Saturated liquid density

The saturated liquid density has been measured by method using pyrex glass floats. Figure 3 shows a schematic diagram of the apparatus. The pyrex glass floats and sample liquid were put in the high pressure glass vessel, and the whole setup was immersed into a thermostat bath. Their behaviour was observed carefully controlling temperature of the bath. The temperature required to hold the float freely suspended in the liquid was measured. The method of temperature measurement is the same as mentioned above in Sec. 2.1. The density of the float was determined to be accurate to ± 1 kg/m³ at room temperature condition, and was corrected with respect to the thermal expansion deformation of glass. The experimental uncertainties of temperature and density were estimated ± 20 mK and ± 3 kg/m³, respectively.
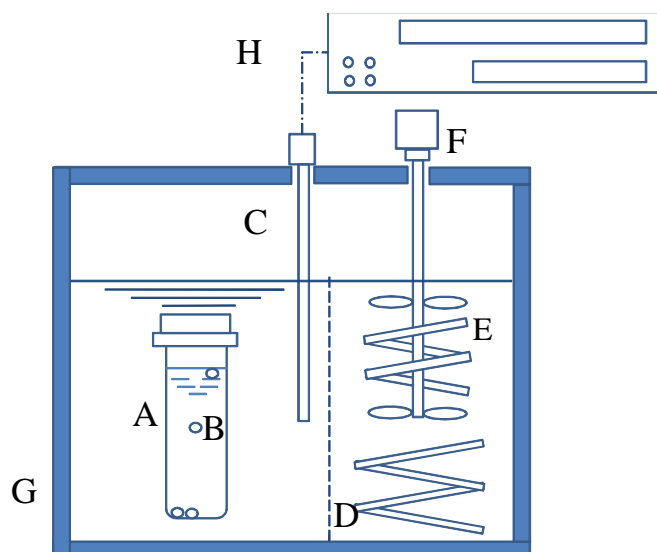
A: Optical cell   B: Pyrex glass floats   C: Platinum resistance thermometer   D: Heater
E: Cooler   F: Stirrer   G: Thermostated bath   H: Thermometer bridge
Figure 3: Schematic diagram of the apparatus for Saturated liquid density the method using pyrex glass floats

2.4 Sample

The purity of the HCFO-1224yd sample used in the experiments was 98.4 %(Z isomer/E isomer=91/9). The water content was less than 5 wtppm.

3. RESULTS

3.1 Vapor-liquid coexistence curve near the critical region

The experimental temperature-density data along the vapor-liquid coexistence curve near the critical region are given in Table 1 and Figure 4. Totally 7 measurements in the range from 371 to 675 kg/m³ were obtained between the temperature of 427 K and the critical temperature.

Table 1: Experimental results of vapor-liquid coexistence curve near the critical region

T (K)	ρ (kg/m³)	T (K)	ρ (kg/m³)
427.71	371.20	429.17	530.18
428.25	414.70	429.02	600.00
428.66	417.01	427.66	674.13
429.19	469.29		
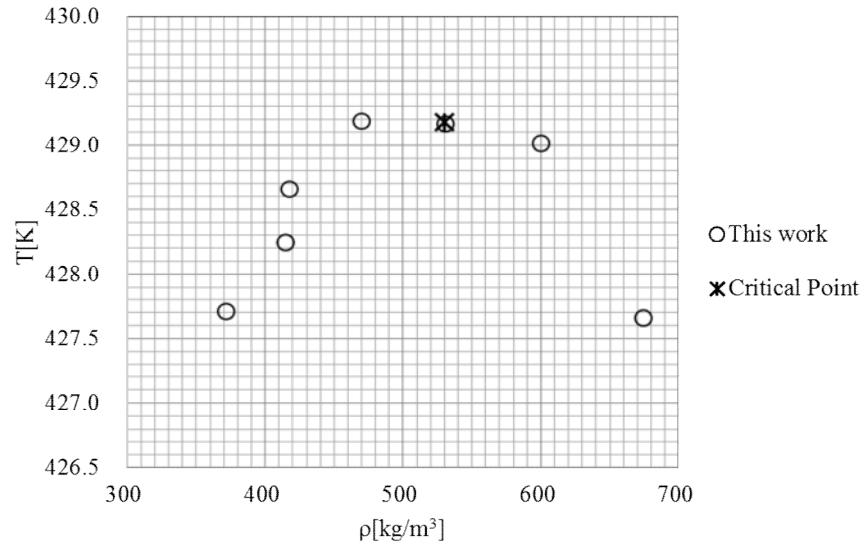
Figure 4: Experimental results of vapor-liquid coexistence curve near the critical region

3.2 Vapor pressure and PVT properties

Vapor pressure and PVT properties were measured along 7 isochores. 201 PVT property measurements were obtained in the range of temperature from 313 to 473 K, of pressure from 0.2 to 9.5 MPa, and density from 51 to 793 kg/m^3. These results are given in Table 2. Figures 5 and 6 show the distribution of the present vapour pressure and PVT properties data.

Figure 5: Experimental results of vapor pressure and PVT properties

Figure 6: Experimental results of vapor pressure and PVT properties
(Filled symbols: the vapor-liquid two phase state)

Table 2: Experimental results of vapour pressure and PVT properties
(Asterisks: the vapor-liquid two phase state)

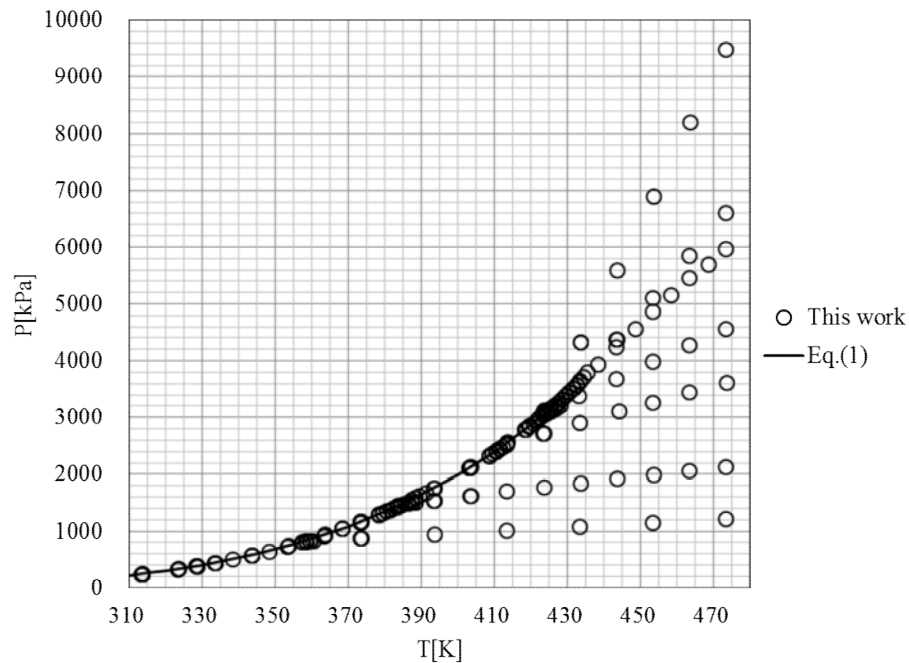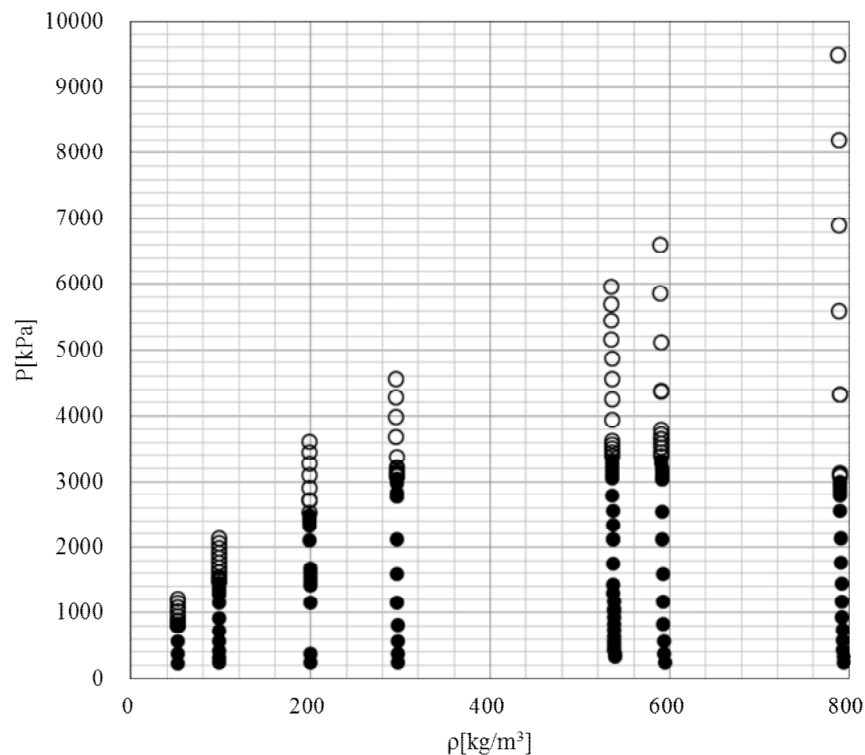| T (K)	P (kPa)	ρ (kg/m³)		T (K)	P (kPa)	ρ (kg/m³)	
313.428	243.62	51.55	*	373.261	1155.7	97.61	*
328.413	381.95	51.51	*	378.198	1290.6	97.58	*
343.374	574.33	51.48	*	378.228	1294.2	97.58	*
357.144	808.09	51.45	*	379.276	1319.1	97.58	*
357.423	811.98	51.45	*	379.367	1321.0	97.58	*
358.506	822.71	51.44		380.222	1348.1	97.58	*
359.260	826.19	51.44		380.228	1352.5	97.58	*
359.408	826.02	51.44		381.278	1376.2	97.57	*
360.232	830.94	50.44		382.120	1404.6	97.57	*
373.217	881.17	51.41		383.224	1431.4	97.56	*
373.260	880.95	51.41		383.307	1438.2	97.56	*
373.580	880.30	51.41		384.285	1460.8	97.56	*
393.447	952.46	51.36		386.164	1492.6	97.55	
413.239	1021.03	51.31		386.319	1490.7	97.55	
433.259	1084.38	51.26		387.249	1501.1	97.54	
453.222	1154.01	51.20		387.355	1501.6	97.54	
473.220	1219.10	51.25		388.170	1509.9	97.54	
				388.282	1507.0	97.54	
313.420	247.4	97.88	*	393.216	1548.3	97.51	
323.313	331.0	97.84	*	393.371	1546.8	97.51	
333.407	434.8	97.79	*	403.206	1629.9	97.47	
343.411	570.3	97.75	*	403.389	1629.2	97.47	
353.128	737.2	97.70	*	413.246	1705.5	97.42	
363.103	924.0	97.65	*	423.411	1779.6	97.37	

Table 2: Experimental results of vapor pressure and PVT properties (continue)
(Asterisks: the vapor-liquid two phase state)

T (K)	P (kPa)	ρ (kg/m³)		T (K)	P (kPa)	ρ (kg/m³)	
433.406	1850.2	97.32		427.271	3187.3	295.17	
443.370	1922.6	97.27		428.076	3216.8	295.16	
453.412	1995.7	97.22		433.066	3376.9	295.09	
463.200	2066.8	97.17		443.166	3684.9	294.94	
473.300	2137.3	97.12		453.119	3988.0	294.79	
				463.203	4283.3	294.64	
313.353	247.8	199.43	*	473.173	4570.2	294.49	
328.535	388.2	199.29	*				*
373.198	1157.2	198.87	*	323.352	338.8	538.26	*
383.235	1426.6	198.78	*	328.295	390.5	538.14	*
385.208	1488.2	198.76	*	333.298	448.5	538.02	*
387.213	1555.2	198.74	*	333.398	448.0	538.01	*
389.290	1621.9	198.72	*	338.242	510.1	537.89	*
391.090	1680.5	198.70	*	343.434	582.4	537.77	*
403.250	2114.3	198.59	*	348.318	649.9	537.64	*
408.352	2325.9	198.54	*	353.367	745.5	537.52	*
409.294	2369.5	198.53	*	358.178	837.6	537.39	*
410.283	2411.9	198.52	*	363.398	940.3	537.26	*
410.283	2411.9	198.52	*	368.139	1049.7	537.14	*
410.306	2412.4	198.52	*	368.166	1050.0	537.14	*
410.445	2416.0	198.51	*	368.186	1050.8	537.14	*
411.193	2449.2	198.51	*	373.250	1170.2	537.01	*
411.288	2455.0	198.51	*	378.244	1302.3	536.88	*
412.202	2492.8	198.50	*	383.178	1441.7	536.76	*
412.288	2496.5	198.50	*	393.296	1760.9	536.49	*
413.308	2529.6	198.49		402.947	2117.0	536.24	*
423.214	2726.3	198.39		403.251	2126.3	536.23	*
423.324	2724.1	198.39		408.423	2339.0	536.10	*
423.342	2725.2	198.39		413.270	2557.0	535.97	*
433.185	2911.5	198.29		418.352	2795.8	535.83	*
443.893	3110.7	198.18		423.326	3056.9	535.70	*
453.160	3274.8	198.09		424.382	3109.0	535.67	*
463.289	3449.2	197.99		425.355	3165.5	535.65	*
473.360	3621.4	197.89		426.388	3220.4	535.62	*
				427.419	3274.8	535.59	*
313.409	247.3	296.78	*	428.406	3332.6	535.57	
328.465	388.7	296.57	*	429.456	3399.6	535.54	
343.539	581.3	296.37	*	430.219	3452.6	535.52	
358.261	828.3	296.16	*	431.505	3519.4	535.48	
373.108	1166.1	295.96	*	432.354	3571.8	535.46	
388.106	1592.6	295.74	*	433.277	3635.5	535.44	
403.049	2120.5	295.53	*	438.311	3943.8	535.30	
418.224	2786.7	295.31	*	443.181	4253.1	535.17	
418.339	2787.7	295.31	*	448.424	4564.5	535.03	
419.233	2839.0	295.29	*	453.261	4866.8	534.90	
422.264	2991.1	295.25	*	458.268	5168.2	534.76	
423.181	3039.3	295.23	*	463.245	5456.9	534.62	
423.202	3040.4	295.23	*	468.366	5708.0	534.48	
424.230	3084.8	295.22		473.197	5969.6	534.35	
424.241	3086.8	295.22					*
425.201	3117.9	295.21		313.295	247.3	593.69	*
425.234	3122.5	295.20		328.316	386.9	593.28	*
426.251	3154.4	295.19		343.407	579.4	592.87	*

Table 2: Experimental results of vapor pressure and PVT properties (continue)
(Asterisks: the vapor-liquid two phase state)

T (K)	P (kPa)	ρ (kg/m3)		T (K)	P (kPa)	ρ (kg/m3)	
358.320	835.3	592.46	*	323.466	337.4	792.96	*
373.289	1167.7	592.04	*	333.517	447.6	792.59	*
388.338	1592.9	591.61	*	343.542	583.5	792.22	*
403.249	2124.3	591.18	*	353.498	747.2	791.86	*
413.220	2551.7	590.89	*	363.485	943.5	791.48	*
423.262	3049.4	590.60	*	373.573	1177.1	791.10	*
423.305	3049.2	590.60	*	383.520	1449.1	790.73	*
424.289	3103.8	590.57	*	393.514	1768.3	790.35	*
425.405	3157.5	590.54	*	403.529	2135.6	789.96	*
426.342	3211.4	590.51	*	413.542	2567.1	789.57	*
427.347	3271.6	590.48	*	418.440	2800.8	789.38	*
428.309	3324.8	590.45		419.551	2855.1	789.34	*
429.327	3391.1	590.42		420.488	2901.1	789.30	*
430.309	3454.8	590.39		421.465	2952.6	789.26	*
431.382	3524.9	590.36		421.608	2957.8	789.26	*
432.345	3591.9	590.33		422.232	2991.3	789.23	*
433.258	3661.3	590.30		422.448	3007.6	789.22	*
433.317	3662.2	590.30		423.250	3093.5	789.19	
434.344	3729.8	590.27		423.410	3118.1	789.19	
435.340	3802.7	590.24		423.479	3134.5	789.18	
443.277	4379.2	590.01		433.468	4338.3	788.79	
443.405	4383.7	590.00		433.563	4333.4	788.79	
453.293	5113.8	589.71		443.371	5604.0	788.40	
463.272	5858.3	589.41		453.453	6899.2	787.99	
473.241	6614.9	589.11		463.377	8197.1	787.60	
				473.286	9495.7	787.19	
313.436	249.3	793.32	*				

3.3 Saturated liquid density

Saturated liquid densities were obtained in the temperature range from 263 to 325 K. The measurements had been conducted by the method using pyrex glass floats. These results are given in Table 3. Also 2 saturated liquid density was determined as the intersection points of PVT property data in the compressed liquid region and vapor pressure. The uncertainties of the analyzing points for saturated density and temperature were estimated within 0.4 % and 0.5 K. This result is also given in Table 5 and Figure 7.

Table 3: Experimental results of saturated liquid densities

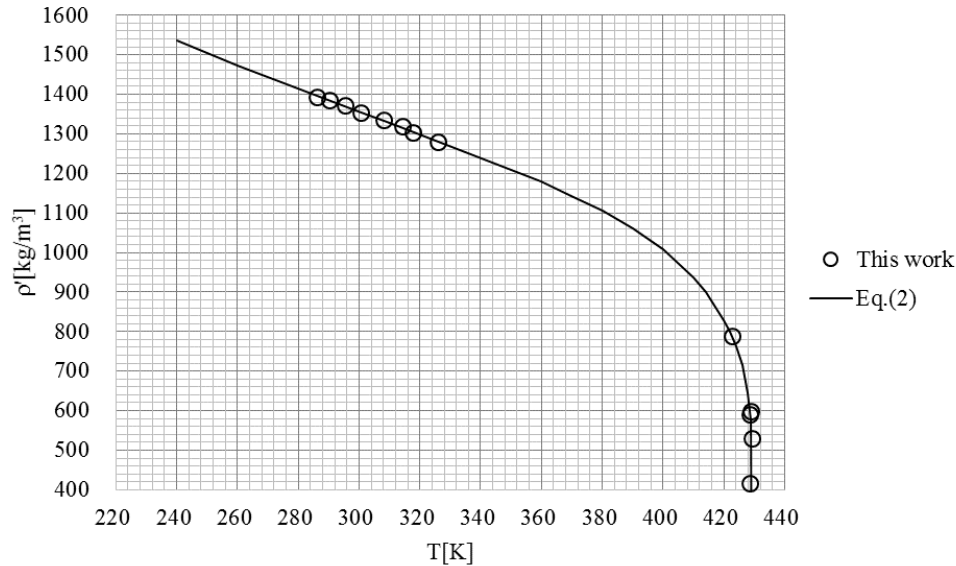| buoy		cont. vol.	
T (K)	ρ' (kg/m³)	T (K)	ρ' (kg/m³)
286.26	1395	428.50	590
290.26	1384	422.56	789
295.44	1371		
300.55	1354		
308.11	1336		
314.18	1320		
317.59	1304		
325.87	1281		

Figure 7: Experimental results of saturated liquid density

4. DISSCUSION

4.1 Critical parameters

On the basis of measurements of the density-temperature relation along the vapor-liquid coexistence curve in the range densities from 469.2 to 600.0 kg/m^3 near the critical point, the critical density was determined by the observation of disappearance of the vapor-liquid interface and of the intensity of critical opalescence. The critical density was determined as follows:

$$\rho_c = 530 \pm 5 \text{kg/m}^3$$

The critical temperature can be determined as the saturation temperature corresponding to the critical density. A shown in Table 1, the saturation temperature in the density range between 469.2 and 600.0 kg//m^3 agree with each other within uncertainty of temperature measurements, and that of density of 530.0 kg/m^3, closest the critical density, was 429.17 K. Therefore, we determined the critical temperature as follows:

$$T_c = 429.18 \pm 0.05 \text{K}$$

The critical pressure was determined by extrapolation of the vapor pressure measurements to the critical temperature as follows:

$$P_c = 3.380 \pm 0.005 \text{MPa}$$

4.2 Vapor pressure

The correlation of vapor pressure was developed. This equation is given by

$$\ln P_{vpr} = (A_0\tau + A_1\tau^{1.5} + A_2\tau^{2.5} + A_3\tau^5)/T_r \tag{1}$$

where $\tau=(1-T/T_c)$, A_0, A_1, A_2 and A_3 are fitting parameters. The parameters of equation (1) were determined by the least square fitting based on the present data. The best values for the parameters and root mean square deviations are given in Table 4. Figure 8 shows the vapor pressure deviations from equation (1).
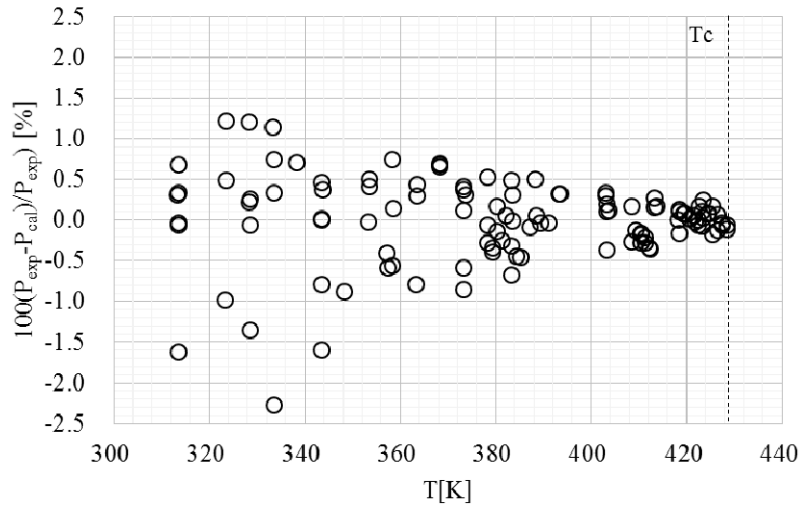
Figure 8: Deviation of vapor pressure measurements from eq. (1)

4.3 Saturated liquid density

The correlation of saturated liquid density was developed. This equation is given by

$$\rho'/\rho_c = 1 + B_0\tau^{1/3} + B_1\tau^{2/3} + B_2\tau + B_3\tau^{4/3} \tag{2}$$

where $\tau = (1 - T/T_C)$ and B_0, B_1, B_2 and B_3 are fitting parameters. These parameters of equation (2) were determined by the least square fitting based on the present data. The best values for the parameters and root mean square deviations are given in Table 4. Figure 9 shows the saturated liquid density deviation from equation (2).

Table 4: Numerical constants of coefficients in equations (1) and (2)

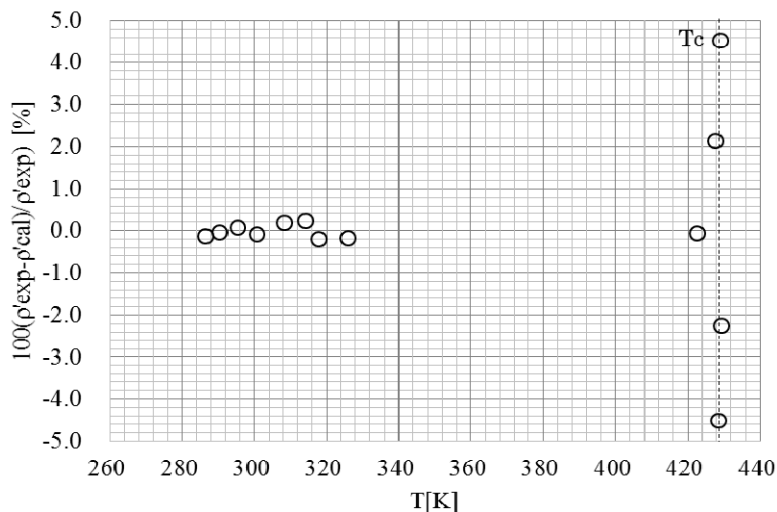|		
	A_0	-7.6720
	A_1	1.9095
Eq.(1)	A_2	-2.6381
	A_3	-5.5113
	RMS Dev.(%)/Number of data points	0.51 / 116
	B_0	0.51475
	B_1	9.6947
Eq.(2)	B_2	-18.564
	B_3	12.138
	RMS Dev.(%)/Number of data points	1.97 / 13
T_C	(K)	429.18
P_C	(MPa)	3.380
ρ_c	(kg/m^3)	530

Figure 9: Deviation of saturated liquid density measurements from eq. (2)

5. CONCLUSION

The thermodynamic properties data for HCFO-1224yd were determined experimentally. The critical parameters were determined by our present data. The correlations of vapor pressure and saturated liquid density were developed based on the present measurements.

NOMENCLATURE

P	pressure	(MPa, kPa)
ρ	density	(kg/m³)
ρ'	saturated liquid density	(kg/m³)
RMS Dev.	root mean square deviation	
T	temperature	(K)

Subscript

c	critical
r	reduced, as in $T_r = T/T_c$, $P_{vpr} = P_{vp}/P_c$
vp	vapor pressure

REFERENCES

Fukushima, M., Hayamizu, H., Tanaka, T., Otsuka, T., Hashimoto, M. (2015). Development of low-GWP alternative refrigerants, *Proceedings of the 13th Asia Pacific Conference on the Built Environment Next Gen technology to make green building sustainable*, Hong Kong, China.

ACKNOWLEDGEMENT